Cell, Vol. 111, 721–732, November 27, 2002, Copyright ©2002 by Cell Press

Selection of tRNA by the Ribosome Requires a Transition from an Open to a Closed Form

James M. Ogle, Frank V. Murphy IV, Michael J. Tarry, and V. Ramakrishnan[1]
MRC Laboratory of Molecular Biology
Hills Road
Cambridge CB2 2QH
United Kingdom

Summary

A structural and mechanistic explanation for the selection of tRNAs by the ribosome has been elusive. Here, we report crystal structures of the 30S ribosomal subunit with codon and near-cognate tRNA anticodon stem loops bound at the decoding center and compare affinities of equivalent complexes in solution. In ribosomal interactions with near-cognate tRNA, deviation from Watson-Crick geometry results in uncompensated desolvation of hydrogen-bonding partners at the codon-anticodon minor groove. As a result, the transition to a closed form of the 30S induced by cognate tRNA is unfavorable for near-cognate tRNA unless paromomycin induces part of the rearrangement. We conclude that stabilization of a closed 30S conformation is required for tRNA selection, and thereby structurally rationalize much previous data on translational fidelity.

Introduction

Translation of mRNA into protein involves a compromise between speed and accuracy, with error frequencies estimated to be as low as 1×10^{-4} (Kurland et al., 1996). The selection by the ribosome of substrate aminoacyl-transfer RNAs (aa-tRNAs) for incorporation of amino acids into a growing peptide chain depends on base complementarity between the codon on mRNA and the anticodon on tRNA. However, near-cognate tRNAs, which differ from the correct or cognate tRNAs by a single, subtle mismatch in codon-anticodon base-pairing, cannot be accurately discriminated against on the basis of differences in the free energy of base-pairing alone.

The proposal of a "decoding site" in the 30S subunit that distinguishes between correct and incorrect tRNAs arose from the discovery that streptomycin increases the error rate of protein synthesis (Davies et al., 1964). In analogy with enzymes, this site would discriminate against incorrect tRNAs due to suboptimal shape and interactions. A second idea is that translational accuracy is the result of a kinetic proofreading mechanism (Hopfield, 1974; Ninio, 1975), in which the free energy difference between the binding of correct and incorrect tRNAs can be exploited twice, to give as much as the product of the selectivities at each step. Aminoacyl tRNA is initially presented to the ribosome as part of a ternary complex with EF-Tu and GTP. Correct codon-anticodon interactions trigger the hydrolysis of GTP by EF-Tu. After GTP hydrolysis, the aminoacyl end of tRNA is released by EF-Tu, at which point it can swing into the A site of the peptidyl transferase center, triggering peptide bond formation, or it has a second chance to dissociate from the ribosome. Thus, there are two dissociation steps that are separated by irreversible GTP hydrolysis, so that differences in base-pairing free energy of cognate and near-cognate tRNA were considered sufficient to explain the accuracy of tRNA selection.

However, recent findings suggest that this view is too simple. The NMR structure of the error-inducing aminoglycoside paromomycin bound to a fragment of A site 16S RNA led to the proposition that the antibiotic might stabilize the decoding site in a conformation which specifically recognizes the codon-anticodon duplex (Fourmy et al., 1996). Kinetic studies showed that cognate tRNA, or paromomycin with near-cognate tRNA, specifically accelerate the rates of GTPase activation and accommodation, further implicating induced fit as a source of selectivity (Rodnina and Wintermeyer, 2001). Moreover, the energetic cost of replacing A:U by a G:U mismatch in double-stranded RNA (Mathews et al., 1999; Xia et al., 1998) is too small to explain even the differences in dissociation rates of cognate and near-cognate tRNAs. This strongly suggests that the ribosome recognizes base-pairing geometry during decoding, thus raising the intrinsic selectivity of each step to the levels required.

Three key bases, G530, A1492, and A1493 (Powers and Noller, 1994), line the floor of the 30S A site (Schluenzen et al., 2000; Wimberly et al., 2000). In the presence of paromomycin, A1492 and 1493 were found to occupy positions in which they might directly interact with the minor groove of the codon-anticodon helix (Carter et al., 2000). The structure of the 30S subunit with A site codon and cognate tRNA anticodon stem loop (ASL) subsequently revealed conformational changes in the 30S, in which A1492, A1493, and G530 interact intimately with the minor groove of the first two codon-anticodon base pairs (Ogle et al., 2001). However, some of the most important questions remained unanswered: is the accuracy of each tRNA selection step compatible with the change in free energy when these interactions involve near-cognate rather than cognate anticodon? How can this discrimination affect the critical steps in tRNA selection, which involve acceleration of forward rates? Finally, how can disparate biochemical and genetic data on translational fidelity be understood in structural terms? To address these issues, we here describe crystal structures of near-cognate 30S-codon-ASL complexes and compare the structures with binding affinity measurements in solution.

Structures of Near-Cognate Anticodon Stem Loops Bound to Codon in the 30S Decoding Center

Crystal structures were determined after soaking the phenylalanine codon UUU and ASLs of near-cognate

[1]Correspondence: ramak@mrc-lmb.cam.ac.uk

Table 1. Summary of Crystallographic Data

Data set	U_6/ASL^{Leu2}	U_6/ASL^{Ser}	U_6/ASL^{Leu2}/ paromomycin	U_6/ASL^{Ser}/ paromomycin
	Data collection			
Beamline	ID14-4	ID14-4	ID14-4	ID14-4
Resolution limit (Å)	3.80	3.65	3.00	3.35
Unit cell				
a,b (Å)	401.84	402.84	400.30	401.60
c (Å)	173.85	174.28	175.50	176.03
No. of observations	456,527	512,952	918,025	863,318
No. of unique reflections	135,995	150,852	272,610	188,834
R_{sym}[a] (%)	8.0 (29.5)	13.7 (50.9)	12.8 (56.4)	16.1 (58.6)
Completeness[a] (%)	99.3 (96.1)	92.4 (88.8)	95.5 (80.1)	92.2 (79.4)
$<I>/<\sigma_I>$[a]	7.0 (1.7)	6.2 (1.9)	7.0 (2.0)	6.1 (2.1)
	Refinement			
Resolution range	200–3.80	200–3.65	500–3.00	100–3.35
Reflections excluded for cross-validation (%)	5	5	5	5
R factor[b] (%)	24.2 (31.2)	26.0 (32.4)	22.7 (27.0)	22.5 (28.4)
σ_A coordinate error[c] (Å)	0.61 (0.69)	0.71 (0.81)	0.56 (0.56)	0.58 (0.63)
Number of non-hydrogen atoms	51,757	51,680	52,275	52,140
Proteins	19,170	19,170	19,170	19,170
RNA	32,585	32,508	32,903	32,820
Metals	2	2	160	108
Deviations from ideality				
R.m.s. deviations in bond lengths (Å)	0.007	0.008	0.006	0.006
R.m.s deviations in bond angles (°)	1.2	1.3	1.2	1.2
Average B factor (Å^2)	97.7	87.0	70.5	93.9

[a] Values for the outermost resolution shell are given in parentheses.
[b] The free R-factor is given in parentheses.
[c] The cross-validated σ_A coordinate error is given in parentheses.

Leu^2 or Ser tRNA into crystals of the *Thermus thermophilus* 30S subunit, both in the presence and absence of paromomycin (Table 1). These ASLs, with anticodons 3′-GAG-5′ and 3′-AGG-5′, respectively, pair to the codon with single G:U mismatches at the first or second positions (whereas the G:U pair at the wobble position is allowed).

Induction of Ordered ASL Binding by Paromomycin

X-ray diffraction by crystals from experiments without paromomycin was limited to 3.6–3.8 Å resolution and the average B factors are elevated. No electron density is observed for either near-cognate ASL, though in the ASL^{Leu2} experiment some weak density is visible for the codon sugar-phosphate backbone (Figure 1A). At this resolution, it is not possible to distinguish between occupancy and disorder; thus, the lack of interpretable ASL density could arise from disordered binding rather than no binding at all. A clear loss of density for G530 and C1054, which move to contact the ASL in the case of cognate binding (Ogle et al., 2001), and a concerted movement of the head domain (see below) are inconsistent with the absence of binding.

In contrast, with paromomycin, the resolution is consistently higher, and density is observed in each case for both the ASL and the codon in the A site (Figure 1B). The overall conformations of both near-cognate ASLs are nearly identical to that of the cognate ASL (Figure 1C). These structures also reveal interactions of A1492, A1493, and G530 with the minor groove of the codon-anticodon helix in conformations very similar to the cognate case, and the characteristic closing of the 30S subunit.

Global Conformational Changes in the 30S

The transitions within the 30S subunit for the cognate and near-cognate structures are shown in Figure 2, and as animations in the Supplemental Data (available at http://www.cell.com/cgi/content/full/111/5/721/DC1). The extent of the movement observed in the crystal is unlikely to correspond to the maximum possible in solution, because the free energy available from the complex formation is used to overcome not only intramolecular, but also lattice forces. Figure 2A compares the effects of binding paromomycin, cognate tRNA, and both together. With antibiotic alone, most differences are comparable to coordinate error (ca. 0.4 Å). The excursion at the beak is an artifact from its flexibility and poor order, and the large change at A1492/3 arises from the antibiotic binding.

Cognate ASL induces a closure of the 30S subunit around the A site, which is enhanced in the additional presence of paromomycin. This movement involves rotations of the head toward the shoulder and the subunit interface and of the shoulder (S4, G530 loop with surrounding regions of 16S RNA and S12) toward the intersubunit space and the h44/h27/platform region (Figure 2A). The movement of the spur occurs in these crystals because it mimics P site tRNA in a neighboring 30S molecule (Carter et al., 2000).

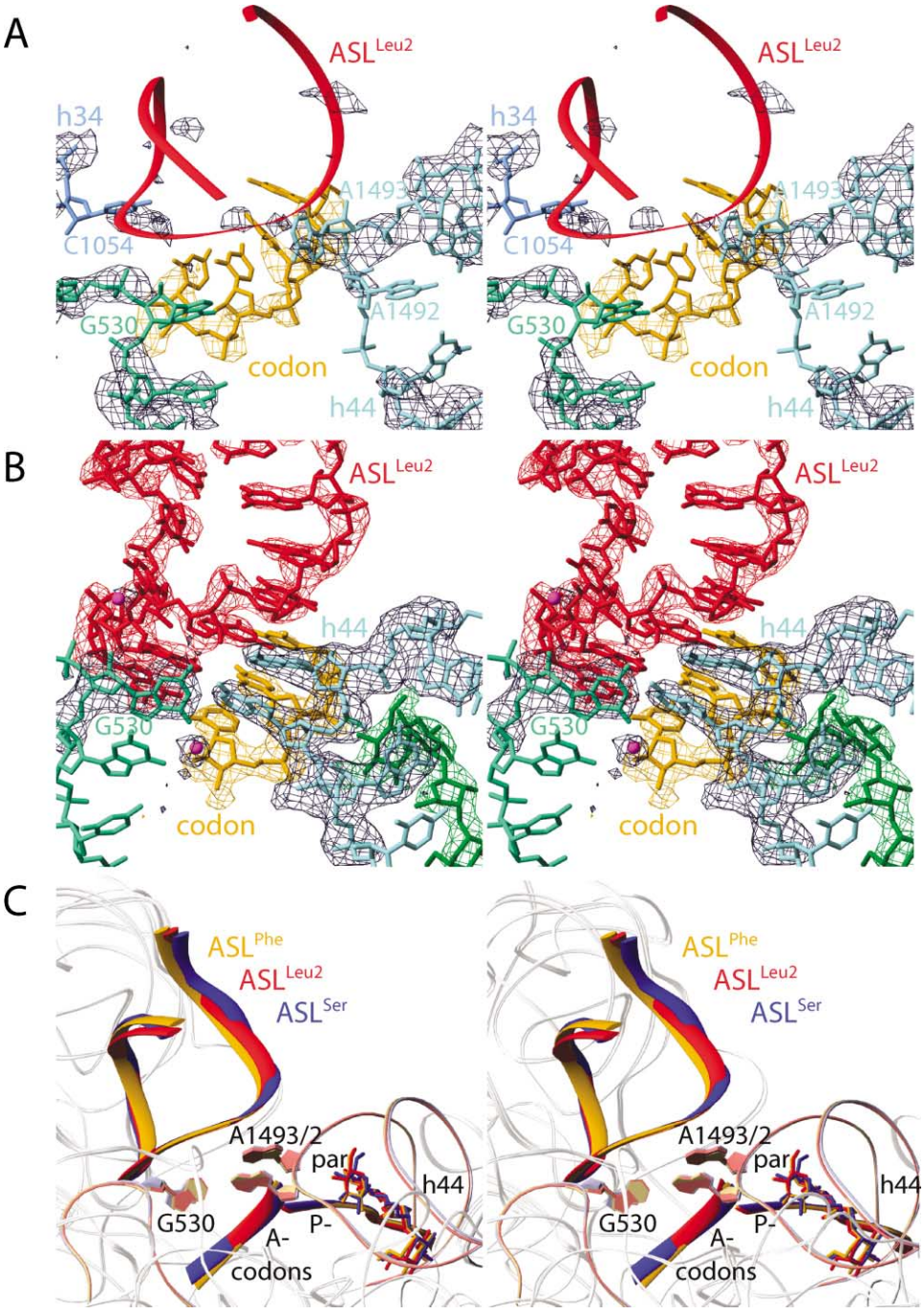

Figure 1. Crystallographic Experiments on the Binding of Near-Cognate ASLs to Codon UUU the 30S Decoding Center

(A and B) ASL^{Leu2}, G:U mismatch at the first codon position. 16S RNA is colored turquoise (530 loop, lower left), light blue (C1054, in helix 34, upper left in A only) and cyan (helix 44, right); codon UUU is gold, ASL^{Leu2} red. Electron density for the codon and ASL is colored corresponding to the atomic models. Density for 16S and Mg^{2+} ions is dark blue. G530, C1054, the nucleotides shown from helix 44, the codon, ASL, paromomycin, Mg^{2+} ions, as well as other nearby portions of the 16S RNA were omitted in the initial refinement runs which generates the density shown here.

(A) Initial omit electron density in the absence of paromomycin. The codon was partially visible only in the $2mF_o$-DF_c density, contoured here at 1.2 σ. A backbone ribbon trace of the ASL^{Leu2} from the structure with paromomycin is shown for comparison with (B). The lack of density for G530, A1492, and A1493 and C1054 indicates disordered movement.

(B) Initial omit mF_o-DF_c difference density in the presence of paromomycin, contoured at 3 σ. Paromomycin with density is shown in green (lower right). Magenta spheres probably represent Mg^{2+} ions.

(C) Overall comparison of the 30S-codon-recognition complexes with cognate ASL^{Phe} (gold, 1IBL, Ogle et al., 2001), ASL^{Leu2} (red), and ASL^{Ser} (blue; mismatch at the second codon position). For each structure, the codon UUU is colored to match the ASL, as are paromomycin and, in the 16S, G530 with the 530 loop (on left), and A1492 and A1493 with helix 44 (on right).

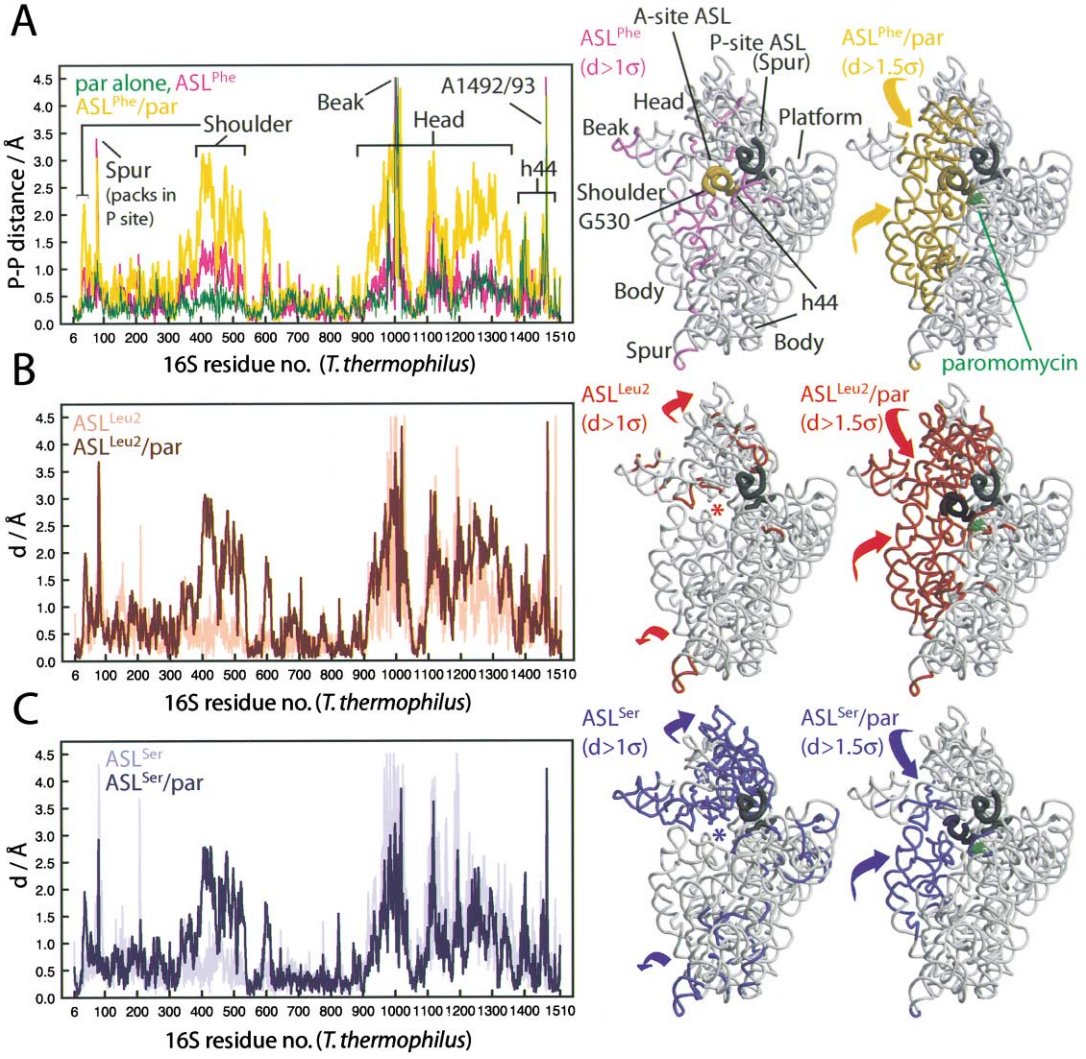

Figure 2. Global Conformational Changes in the 30S Subunit

(A–C) Movements of 16S RNA backbone phosphorus atoms (*T. thermophilus* numbering) after superposition of ASL complexes on the native structure (Wimberly et al., 2000), based upon an analysis of the movement within the 16S RNA with the program ESCET (Schneider, 2002). Regions moving by more than the estimated standard deviation (σ) of the individual atoms (1.5 σ for the ASL complexes with paromomycin) are highlighted in color, and arrows are added to indicate general directions of movement (see Supplemental Data for animations available at http://www.cell.com/cgi/content/full/111/5/721/DC1). With near-cognate ASLs in the absence of paromomycin, no ASL-density appears at the A site (*), though the movement in the head, the perturbation of the surrounding electron density, and the affinity data indicate binding in a disordered manner.

(A) Effect of paromomycin alone (green), cognate ASL^{Phe}(magenta), or both ASL^{Phe} and paromomycin (gold) (Ogle et al., 2001).

(B) ASL^{Leu2} with (dark red) and without (light red) paromomycin. Without paromomycin, the shoulder does not move and the movement of the head is of a different nature, though similar in magnitude.

(C) ASL^{Ser} with (dark blue) and without (light blue) paromomycin. As in (B), 30S closes only with paromomycin, though to a slightly lesser extent.

With near-cognate ASLs (Figures 2B and 2C), the closed 30S is only observed in the presence of the antibiotic. 30S closure is less pronounced in the ASL^{Ser} structure, indicating that it is initiated in particular by the interaction between G530 in the shoulder and A1492 in helix 44, across the minor groove of the second codon-anticodon pair (see below). Without paromomycin, neither near-cognate ASL induces any movement of the shoulder. The head moves to a similar extent as with paromomycin or cognate ASL, but in a different direction (See Supplemental Animations available at above web-site). This movement would be consistent with conformationally disordered binding of the ASL in the A site, without the specific contacts to G530, A1492, and A1493 that appear to initiate movement of the shoulder.

G:U Mismatch at the First Codon Position (ASL^{Leu2})

The crucial difference between the cognate ASL^{Phe} (Ogle et al., 2001) and the near-cognate ASL^{Leu2} with paromomycin (3.0 Å resolution) lies in the type I A-minor motif (Nissen et al., 2001) formed by A1493 with a G:U mismatch instead of an A:U pair at the first codon position

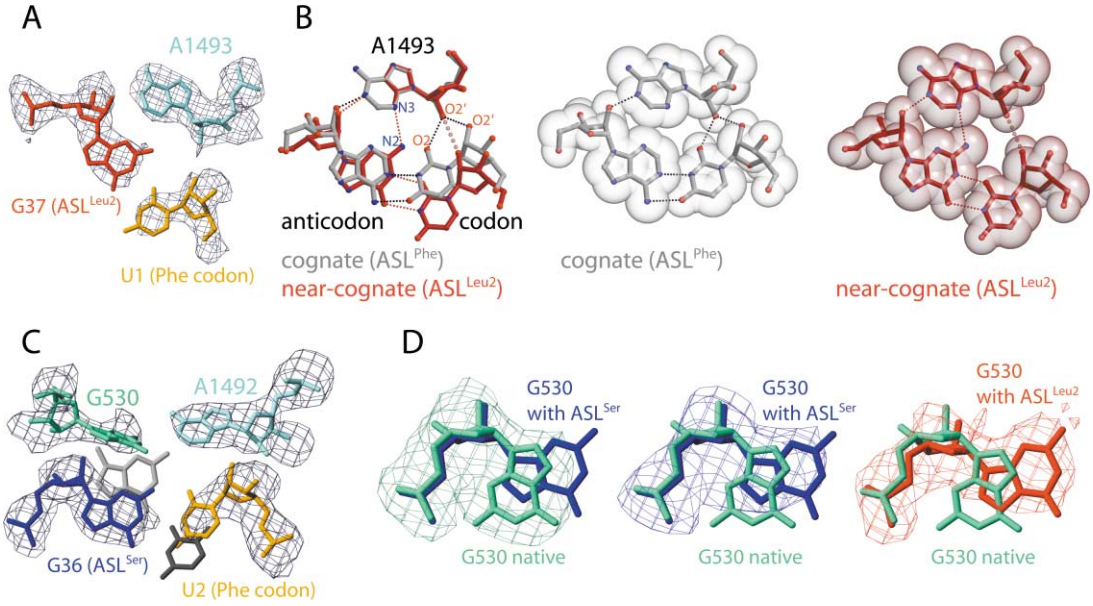

Figure 3. Discrimination at the First Two Codon Positions

(A) Refined $2mF_o$-DF_c electron density (contoured at 1.2 σ) from the ASL^{Leu2}/paromomycin structure for the anticodon-codon G:U mismatch at the first position and A1493.

(B) Superposition of the ASL^{Leu2}/paromomycin structure (dark red), on the corresponding cognate interaction (gray, A:U anticodon-codon base pair; Ogle et al., 2001), in which dashed lines connect hydrogen bond donors and acceptors and the line of larger, transparent red spheres highlights the uncompensated loss of a hydrogen bond caused by separation of A1493 and the codon. The last two images show van der Waals surfaces for the near-cognate and cognate structures, respectively.

(C) Electron density from the ASL^{Ser}/paromomycin structure around the second codon position, showing A1492 and G530. The appropriate position of a guanine base to pair with the refined position of the codon U is shown in light gray; the expected position of a uridine base forming a typical base pair with the refined position of anticodon G is shown in dark gray.

(D) G530 at the second codon position, showing mF_o-DF_c difference electron density (contoured at 3 σ) obtained when the base is omitted from refinement. Superpositions are based upon the 5′-domain of the 16S RNA. In the native structure, the density clearly represents the syn conformation (cyan, Wimberly et al., 2000, G530 in the anti conformation from the ASL^{Ser}/paromomycin structure is superimposed, blue). In the ASL^{Ser}/paromomycin structure (blue), density is weaker, arising from partial disorder due to the G:U mismatch at the second codon position (the native syn structure is superimposed, in cyan). In the ASL^{Leu2}/paromomycin structure (red), the density unambiguously represents the anti conformation.

(Figure 3A). As in any type I A-minor motif with Watson-Crick base pairs containing guanine (G:C or C:G), the N3 of A1493 forms an additional hydrogen bond to the N2 amino group of the anticodon guanine. However, the hydrogen bonding pattern of G:U base-pairing, which involves the uridine O2, displaces the codon U1 away from the minor groove, and thus from A1493, compared to Watson-Crick pairs. The distance between the O2′ atoms of A1493 and the codon U1 (3.4 Å) is greater than in the equivalent interactions with Watson-Crick base pairs previously observed for this motif both in the cognate complex (2.7 Å; Ogle et al., 2001) and in RNA tertiary structure (Doherty et al., 2001; Nissen et al., 2001; Wimberly et al., 2000). Together with the relative orientations of the 2′-OH groups, this implies that U1 and A1493 no longer form any hydrogen bonds. The complementarity of van der Waals surfaces is also lost (Figure 3B). However, there is no room for water between the codon U1 and A1493, so the two 2′-OH groups must nonetheless be desolvated.

G:U Mismatch at Second Codon Position (ASL^{Ser})

In the structure with ASL^{Ser} and paromomycin (3.35 Å resolution), the density for ASL^{Ser} is somewhat less well defined, and the average B factors in the anticodon bases (112 $Å^2$) are higher than in the structures with cognate ASL^{Phe} without or with paromomycin, or ASL^{Leu2} with paromomycin (75 $Å^2$, 61 $Å^2$, and 68 $Å^2$, respectively). The average B factor for all 16S RNA bases is also higher than in other structures containing ASL (89 $Å^2$ versus 66 [$\pm$1] $Å^2$), and is similar to the structures in the absence of paromomycin, in which no ASL density is visible.

Interestingly, the G:U pair, while fitting the density reasonably well, does not refine into the standard wobble geometry (Figure 3C). It is possible that the density represents the spatial average of the G:U pair in two alternative positions, each of which allows the 16S decoding center to interact with one half of the minor groove as shown. In one case, G520 has flipped from the syn to anti conformation but A1492 cannot interact with the codon. In the other case, A1492 and the codon do interact, but a steric clash with the anticodon would prevent the switch of G530 to the anti conformation, and thus its interaction with the anticodon and A1492.

In support of this view, though the electron density for G530 fits the anti conformation best, it is less clearly defined (Figure 3D) than either in the native structure with the unoccupied A site (G530 syn) (Wimberly et al., 2000) or in the codon recognition complexes with ASL^{Phe} and ASL^{Leu2} which have a Watson-Crick A:U pair at this

position (G530 anti). Also, the refined B factor of 126 Å^2 for the guanine ring is significantly higher than the average of all 16S bases (89 Å^2), or the 74 ($\pm$7) Å^2 average for the G530 base from five independent 30S subunit structures in which this base occupies a defined syn or anti conformation. Alternatively, the presence of paromomycin might favor a more Watson-Crick-like geometry of G:U pairing, involving the unusual enol tautomer of G or U, or a bifurcated hydrogen bond (Chen et al., 2000).

Correlation of Structural Results with Measurements of A Site Affinity

In order to relate our structures to differences in free energy, we have measured the equilibrium binding of the cognate and near-cognate ASLs to the A site of 70S ribosomes, in the presence and absence of paromomycin and on both phenylalanine codons, UUU and UUC. 70S ribosomes were used because the structure of the 30S in the crystal more closely resembles the 50S bound form than free 30S subunits (Carter et al., 2000; Wimberly et al., 2000). Affinities were determined by competition of a constant amount of labeled cognate ASL with increasing concentrations of unlabeled cognate or near-cognate ASL. This allows measurements of low affinities arising from the high dissociation rate of near-cognate ASLs. Binding curves are shown in Figure 4 and results are summarized in Table 2.

Compared to cognate ASL^{Phe}, binding of ASL^{Leu2} and ASL^{Ser} with G:U mismatches at the first and second codon positions, respectively, and is reduced by factors of 2.7×10^{-4} and 5.8×10^{-4} (codon UUC, with paromomycin). The corresponding free energy differences of around 18 kJ/mol are significantly higher than the 1–3 kJ/mol (factor of 0.5–0.2) predicted by the thermodynamics of base-pairing for equivalent replacements of A:U by G:U at 0°C (calculated from Mathews et al., 1999; Xia et al., 1998). However, they can be rationalized by the uncompensated loss of hydrogen bonding in the G:U:A1493 interaction in the ASL^{Leu2} structure (Figure 3A). Though such a disruption of contacts is less directly visible in the ASL^{Ser} structure, the reduction in affinity we observe with G:U at the second position strongly suggests that the minor groove interactions of A1492 and G530 selectively stabilize binding of cognate ASL to a similar extent as at the first codon position. This reduction in binding affinity for near-cognate ASL is in good agreement with a case of uncompensated desolvation in enzyme-inhibitor complexes (Bartlett and Marlowe, 1987). Moreover, the effects of mismatches on tertiary interactions involving a type I A-minor motif in the group I intron are at least as large as the free energy differences measured here (Battle and Doudna, 2002).

In contrast to the large effect of replacing A:U by G:U at the first two codon positions, replacing a G:C by a G:U pair at the third ("wobble") position (comparison of cognate binding to UUC versus UUU) reduces affinity by only by a factor of roughly 0.1 (5 kJ/mol). This agrees well with the difference measured for the binding of these two codons to tRNA^{Phe} in the absence of the ribosome (Eisinger et al., 1971; Pongs et al., 1973).

Paromomycin increases the affinity of cognate ASL^{Phe} by a factor of around 15, corresponding to a free energy difference of about 6 kJ/mol. The most clearly visible structural effect of paromomycin in the 30S subunit is the positioning of A1492 and A1493 outside helix 44. These adenines are flexible in the unliganded 30S structure, but become highly ordered when either paromomycin, the cognate codon-ASL complex, or near-cognate codon-ASL with paromomycin are bound to the 30S subunit, as indicated by the appearance of well-defined electron density and an extreme drop in B factors from nearly 200 Å^2 to around 50 Å^2. This suggests that paromomycin lowers the entropic cost of binding ASL by preorganizing these adenines.

In contrast to the cognate case, paromomycin does not enhance the affinity of near-cognate ASL. Superficially, this result appears to contradict the observation of ASL electron density in the presence of paromomycin but not in its absence. However, the roughly equal affinity must be the result of distinct, yet compensating factors. When a cognate codon recognition complex is formed, the total gain in free energy from the interaction between the ribosome and the codon-anticodon minor groove outweighs unfavorable contributions such as desolvation of interacting molecular surfaces, entropic penalties for correct positioning of ligands and binding site, and the enthalpic cost of conformational changes. In the near-cognate case, the minor groove interactions do not appear to be sufficiently strong to drive 30S closure. Nevertheless, the affinity data show that near-cognate ASL alone binds as strongly to the 30S as in the presence of the antibiotic. The crystallographic data indicate that the 30S in this association must be largely in an open conformation, which does not involve movement of the 30S shoulder (see Supplemental Animations available at http://www.cell.com/cgi/content/full/111/5/721/DC1 and Figures 2B and 2C), and in which the ASL and the decoding center retain conformational flexibility, resulting in poorer overall diffraction as well as weak and uninterpretable density.

The thermodynamic balance for near-cognate ASL binding is altered when paromomycin constrains A1492 and A1493 to conformations in which they must closely approach the codon-anticodon minor groove. Though this leads to some unfavorable interactions, the cost of reaching the closed 30S conformation is reduced, because the antibiotic stabilizes A1492 and A1493 in the "bound" conformation. Thus, unlike cognate ASL, which binds with induced fit whether paromomycin is present or not, near-cognate ASL binds to the open 30S without paromomycin, but induces the closed form only in the presence of the antibiotic, resulting in a similar net affinity in the two cases. In rough agreement with our results, previous kinetic experiments (Rodnina and Wintermeyer, 2001) indicated only a small effect of paromomycin on overall affinity of near-cognate tRNA^{Leu2} in ternary complex with EF-Tu and the nonhydrolyzable GTP analog GDPNP. In these studies, the affinity ratio of cognate to near-cognate ternary complexes on the ribosome is about 100:1, which is 3-fold lower than the affinity ratio of ASLs without paromomycin measured here. The small difference may arise partly from an increased entropic cost of positioning A1492 and A1493 at the higher temperature used in the kinetic studies. However, the ratio is still far greater than would arise from codon-anticodon base-pairing, and along with

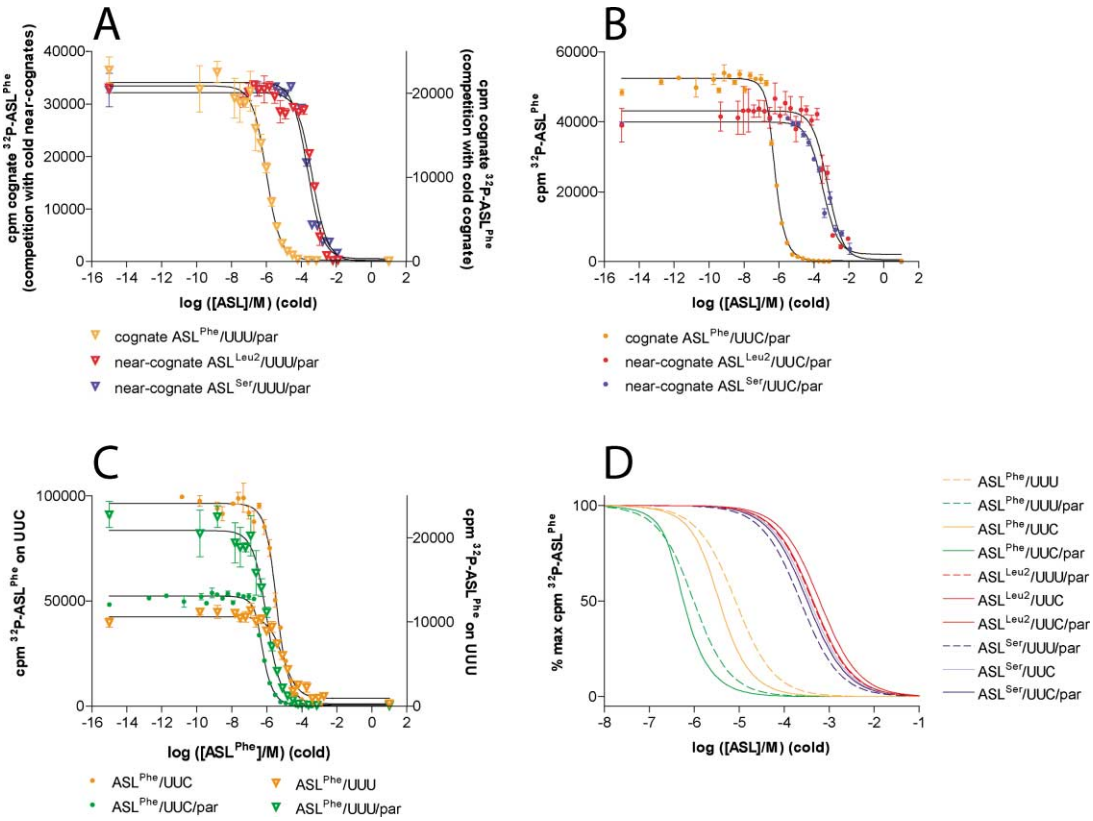

Figure 4. Competition Curves for the Binding of ASLs to the A Site of Programmed, P Site-Blocked 70S Ribosomes (Triplicate Samples, Bars Represent the Standard Error of the Mean)

(A) Cognate ASL^{Phe} (gold), and the near-cognate ASL^{Leu2} (red), and ASL^{Ser} (blue) in the presence of paromomycin, on codon UUU.

(B) As (A), but on codon UUC.

(C) Comparison of cognate ASL^{Phe} with paromomycin (green) and without paromomycin (gold), on codons UUC (filled circles) and UUU (open triangles).

(D) Comparison of normalized nonlinear regression curves from all experiments.

footprinting data (Powers and Noller, 1994), supports the view that the minor groove interactions are involved even in the initial recognition of cognate anticodon in the EF-Tu ternary complex.

Implications for tRNA Selection by the Ribosome

Sources of Discrimination

For any given codon in the A site, the ribosome must be able to distinguish cognate tRNA from all others, in a sequence-independent manner. Traditionally, it was thought that A:U and G:U pairs are distinguished on the basis of their free energies of association, amplified by kinetic proofreading. However, this affinity difference has tended to be overestimated by at least an order of magnitude in studies addressing the translational selectivity mechanism, where it is most often cited as 2–3 kcal/mol (i.e., roughly 8–13 kJ/mol), corresponding to a discrimination capacity of around 1:100 (e.g., Pape et al., 1999; Thompson and Dix, 1982; Thompson and Stone, 1977). Because the selectivity measured on the ribosome in kinetic studies was also ca. 1:100 (in each of the two selection steps), it was suggested that the ribosome equally stabilizes cognate and near-cognate tRNA and thus does not provide additional discrimination over that inherent in codon-anticodon base-pairing in solution (Rodnina and Wintermeyer, 2001). However, the original experiments on affinity ratios in base-pairing (Grosjean et al., 1978; Uhlenbeck et al., 1971) did not directly measure the inherent energetic cost of a single G:U mismatch with respect to an A:U pair. More recent, comprehensive work on the thermodynamics of base-pairing in RNA suggests that this cost is actually much smaller and could reduce affinity by at most a factor of 5–10 in the temperature range 0–37°C (Mathews et al., 1999; Xia et al., 1998). This is too low to account for the accuracy of translation, even with efficient kinetic proofreading. We demonstrate the involvement of two further sources of selectivity in decoding: shape recognition and induced fit.

Discrimination on the Basis of Geometry

The pattern of hydrogen bond acceptors and the overall shape of the minor groove allows recognition of Watson-Crick pairs in a sequence-independent manner (Seeman et al., 1976). 16S RNA bases A1492, A1493, and G530 use this feature to identify cognate tRNA by close contacts to the first two codon-anticodon base pairs. With near-cognate tRNA, the shape of the non-canonical codon-anticodon base pair leads to unsatisfied hydrogen-

Table 2. Summary of A Site Binding Affinity Data

Absolute affinities[1]			
A site codon	ASL^{Phe}	ASL^{Leu2}	ASL^{Ser}
UUU			
log (K_d/M)	−5.12 (±0.01)	n.d.	n.d.
K_d/M	7.6×10^{-6}	n.d.	n.d.
UUU + paromomycin			
log (K_d/M)	−6.24 (± 0.07)	−3.65 (± 0.05)	−4.07 (± 0.06)
K_d/M	5.7×10^{-7}	2.2×10^{-4}	8.5×10^{-5}
UUC			
log (K_d/M)	−6.07 (± 0.03)	−3.66 (± 0.09)	−3.82 (± 0.09)
K_d/M	8.6×10^{-7}	2.2×10^{-4}	1.5×10^{-4}
UUC + paromomycin			
log (K_d/M)	−7.30 (± 0.03)	−3.73 (± 0.09)	−4.07 (± 0.06)
K_d/M	5.0×10^{-8}	1.9×10^{-4}	8.6×10^{-5}

Comparison of Watson-Crick vs. G:U pairing		$\Delta\Delta G_{(273\ K)}$/(kJ/mol)[1]
1st codon position A:U vs. G:U[2]	$K_d(ASL^{Phe})/K_d(ASL^{Leu2})$	
on UUC	3.9×10^{-3}	12.6 (± 0.5)
on UUU + paromomycin	2.6×10^{-3}	13.5 (± 0.5)
on UUC + paromomycin	2.7×10^{-4}	18.7 (± 0.5)
2nd codon position A:U vs. G:U[2]	$K_d(ASL^{Phe})/K_d(ASL^{Ser})$	
on UUC	5.7×10^{-3}	11.7 (± 0.5)
on UUU + paromomycin	6.8×10^{-3}	11.3 (± 0.5)
on UUC + paromomycin	5.8×10^{-4}	16.9 (± 0.4)
3rd codon position G:C vs. G:U[3]	K_d(UUC)/K_d(UUU)	
ASL^{Phe}	1.1×10^{-1}	5.0 (± 0.2)
ASL^{Phe} + paromomycin	8.7×10^{-2}	5.5 (± 0.4)

Effect of paromomycin on cognate ASL^{Phe}		$\Delta\Delta G_{(273\ K)}$/(kJ/mol) [1]
	$K_d(ASL^{Phe})/K_d(ASL^{Phe}$ + paromomycin)	
on UUU	13	−5.9 (± 0.4)
on UUC	17	−6.5 (± 0.2)

[1] Standard errors of (or derived from) the best fit values for log(K_d/M) are given in parentheses; samples were prepared in triplicate; n.d. - not determined.
[2] No hydrogen bond is lost in the codon-anticodon base pair.
[3] One hydrogen bond is lost in the codon-anticodon base pair.

bonding potential or steric clashes within these interactions. Geometry is the most effective criterion for discrimination against all but cognate tRNA. Virtually all non-canonical base pairs contain stabilizing hydrogen bonds, often the same number as Watson-Crick pairs. The importance of Watson-Crick hydrogen bonding is that it also determines the relative orientation of the two interacting bases and hence the geometry of the minor groove, allowing distinction of different, but comparably stable base pairs.

These conclusions provide a clear structural rationale for the wobble hypothesis and the fact that degeneracy within the genetic code is confined to the third position of the codon (Crick, 1966). Previous work on wobble pairing emphasized the role of tRNA, but it is clear from our structures and affinity measurements that the ribosome does not monitor minor groove geometry closely at this position. Therefore, discrimination against G:U and similar pairs is relaxed, because it truly does arise mainly from base-pairing energy differences (though some base pairs, e.g., those with greater overall width, will be sterically excluded).

Roles of Induced Fit

The induced fit required for the discriminating interactions at the minor groove of the codon-anticodon helix is important in various ways. In order to maximally exploit the potential for discrimination by shape, interactions must be as extensive as possible. However, without induced fit, the multiple contacts which enclose the codon and anticodon in the A site would sterically hinder access of the ligands (see also Herschlag, 1988). Because the cost of stabilizing the closed 30S relative to the open form must be derived from the energy of interaction with the codon-anticodon complex, induced fit also allows maximization of contacts without increasing the affinity of cognate tRNA to unreasonably high values, which would limit its rate of release for translocation to the P site. Finally, because the interaction energy with the cognate codon-anticodon minor groove drives movement within the ribosome, distant sites on the ribosome- or bound EF-Tu can detect the presence of a cognate tRNA in the decoding center on the basis of conformational signals, which are not generated when near-cognate tRNA occupies the decoding center.

An Integrated View of the Decoding Mechanism

GTPase activation and accommodation are usually thought of as separate steps in tRNA selection, connected with initial selection and proofreading, respectively. Yet cognate tRNA and paromomycin each accelerate both of these steps (Rodnina and Wintermeyer,

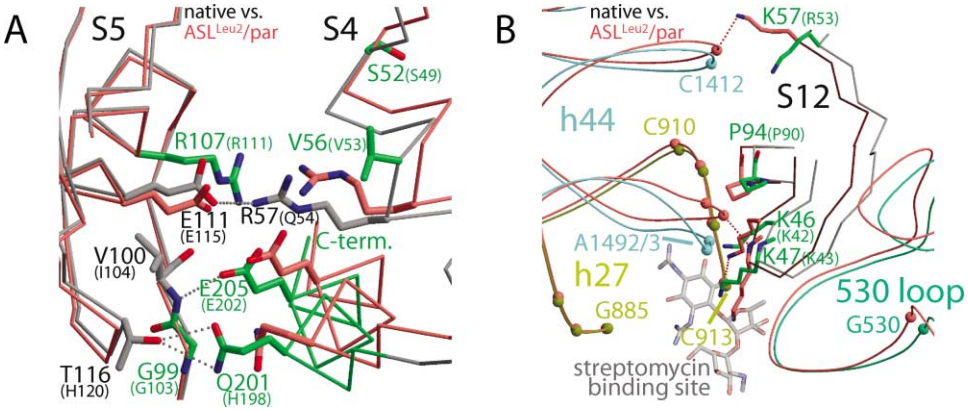

Figure 5. Details of Movements at the S4-S5 Interface and the Region around S12

E. coli numbering is used for RNA residues and in parentheses for protein residues.

(A) Proteins S4 and S5, on the back of the subunit body/shoulder region, move apart due to 30S closure. Based on rigid phosphorus atoms in the 16S RNA identified using ESCET, the ASL^{Leu2}/paromomycin structure (red) is superimposed on the native structure (gray), in which known mutations causing the error-prone ram phenotype are marked green.

(B) The same structure comparison as in (A), showing the formation of contacts between protein S12, and helices 44 and 27 of 16S RNA due the closing rearrangement in the body. Mutations that cause hyperaccurate translation or modulate streptomycin sensitivity are marked green. Streptomycin (from the superimposed 30S complex, pdb-code 1FJG, Carter et al., 2000) is shown for reference.

Please see Supplemental Data for animation of these changes (available at http://www.cell.com/cgi/content/full/111/5/721/DC1).

2001). This suggests that these two steps are part of a concerted process. We show here that cognate tRNA and paromomycin each also promote the closing of the 30S subunit, involving the rearrangement of the shoulder with respect to the rest of the body of the subunit. Our data can rationalize previous work on tRNA selection if we assume that the closed form of the 30S represents a "productive" state (cf. Rodnina and Wintermeyer, 2001), which accelerates both the rate of GTPase activation and accommodation (see below), whereas open forms, which are favored when the A site is empty or contains a near-cognate anticodon, will be inactive in tRNA selection. Thus, the transition to the closed form is important for decoding, rather than the net affinity of the ASL. The specificity available to the ribosome for distinguishing codon-anticodon base pairs by minor groove geometry is thus represented by the energy difference between the cognate and near-cognate ASL complexes with the closed 30S conformation, which can be measured only in the presence of paromomycin. Without the antibiotic, near-cognate tRNA binds to the open form while cognate tRNA binds to the closed form. A direct thermodynamic comparison between the two is therefore not appropriate because nonequivalent conformational states of the 30S subunit are involved. The effective specificity is therefore much higher than would be inferred simply from affinity ratios in the absence of paromomycin.

Structural Aspects of Forward Rate Acceleration

Our structural analysis of the various 30S codon-anticodon recognition complexes indicates that the closing movement of the 30S is initiated by the formation of the ribosomal contacts to the codon-anticodon minor groove. The structure with a G:U mismatch at the first codon position (Figure 3) not only rationalizes reduced ASL affinity (or relative stability of the closed 30S conformation) at equilibrium, but also directly suggests how the rate of the conformational change could be affected. In the cognate case, A1493 forms three hydrogen bonds to the A:U codon-anticodon base pair; two of which are between the A1493 ribose and the codon. However, the A1493 ribose can contact the codon prior to interaction of the base with the anticodon (Figures 2, 3A, and 3B). Interactions to a cognate base pair can thus compensate for desolvation of A1493 progressively, avoiding high activation barriers (cf. Lim and Curran, 2001) by first replacing hydrogen bonds to water in the A1493 ribose, and only afterward in the base. In contrast, in the G:U:A1493 A-minor motif, the A1493 ribose and codon U do not interact, though their desolvation is sterically required. In order to form the two hydrogen bonds to the anticodon G, A1493 must therefore pass though a high-energy state in which both the ribose and the base are fully desolvated, resulting in a higher activation barrier. Paromomycin, on the other hand, accelerates the induced fit to near-cognate tRNA by partially inducing the associated 30S rearrangements independently of the codon-anticodon interaction. Thus, although paromomycin and cognate tRNA lower the activation barrier in different ways, the result is an acceleration of the transition to the closed form in both cases.

Relationship of the Closed Form to GTPase Activation and Accommodation

The orientation of the ASL in the closed 30S subunit corresponds to the accommodated state of tRNA in the 70S (Yusupov et al., 2001), suggesting that this position is favored in the absence of constraints. Initially, however, the tRNA is not free to rotate into the accommodated state because its aminoacyl end is bound to EF-Tu. Instead, the ribosome-ternary complex assembly must experience strain, leading to conformational rearrangements in both the 30S and 50S subunits; in particular, helix 44 in the 16S RNA is thought to be flexible (VanLoock et al., 2000). However, a wealth of data also indicates conformational changes in tRNA, around the

D and T-loops (Rodnina et al., 1994; Yarus and Smith, 1995) or within the anticodon stem (Valle et al., 2002). The tRNA could thus channel binding energy derived from the interaction of the ribosome with the codon-anticodon minor groove into a conformational change in EF-Tu that triggers GTP hydrolysis. Interestingly, cryo-EM studies suggest an interaction of the EF-Tu-bound tRNA acceptor arm with protein S12 (Valle et al., 2002), which moves significantly during closure of the 30S subunit. A role of tRNA as a transmitter of signals has been suggested previously because GTP hydrolysis does not occur with fragmented tRNA (Piepenburg et al., 2000). After GTP hydrolysis, the aminoacyl end of tRNA is released from EF-Tu, so that the tRNA can relax from a strained conformation into the accommodated state, possibly accompanied by further subunit closure. During this rotation, proofreading of the GTPase step occurs, because the interactions between the ribosome and the codon-anticodon minor groove must be sufficiently strong to prevent dissociation of the aa-tRNA in the absence of EF-Tu.

Other Aspects of Translational Fidelity

Our assumption that a transition to the closed form is required for tRNA selection has immediate consequences for understanding mutations that affect translational fidelity. Figure 5A shows that the transition to the closed form induced by A site tRNA binding results in a breakage of various polar interactions at the S4/S5 interface. As was noticed earlier (Carter et al., 2000; Clemons et al., 1999), mutations in S4 and S5 that confer the ram phenotype (e.g., deletion of the C-terminal helix in S4) would also disrupt the interface between them. These mutations would thus facilitate the transition to the closed form by removing the cost of breaking these contacts. On the other hand, elements of S12, h44, and h27 are brought closer together in the closed form (Figure 5B), resulting in the formation of contacts between S12 and the ribosomal RNA, e.g., a salt bridge between K57, and the phosphate of C1412 in h44, or between K46 and the phosphate of A913 in h27. Streptomycin, whose location (Carter et al., 2000) is also shown in Figure 5B, would stabilize the closed form, resulting in lower fidelity. Mutations of key residues in S12 would lead to the loss of stabilizing salt bridges with ribosomal RNA. By destabilizing the closed form, these mutations result in streptomycin resistance or dependence and a hyperaccurate phenotype, e.g., mutation of K57 (*E. coli* R53) results in the most hyperaccurate phenotype known (reviewed in Kurland et al., 1996). The simultaneous breaking of contacts at the S4/S5 interface and the formation of contacts in the S12/h44/h27/streptomycin region explains the compensatory effects of ram and streptomycin resistance mutations. Mutations in h27 could similarly modulate fidelity (Lodmell and Dahlberg, 1997) by changing the relative stability of the closed and open forms and the cost of the transition. However, our model does not require the switch in base-pairing within h27 that was proposed for decoding previously (Lodmell and Dahlberg, 1997), since both the open and closed forms have the same 885/912 base-pairing for h27.

The presence of E site tRNA has been shown to lower A site affinity and increase accuracy (Nierhaus, 1990). Since E site tRNA makes extensive contacts with both the 30S and 50S subunits, its presence may increase the cost of the transition from the open to the closed form, thus increasing accuracy. On the other hand, high concentrations of Mg^{2+} may reduce accuracy by displacing A1492/3 to their position outside h44 and thereby favoring the closed form (Glukhova et al., 1975; Ogle et al., 2001).

Similarities with DNA and RNA Polymerases

Polymerases discriminate efficiently between different base pairs of comparable stability by shape recognition, induced fit, and kinetic partitioning in a proofreading step (Cheetham and Steitz, 2000; Kool, 2002; Kunkel and Bebenek, 2000). Parallels between the tRNA selection pathway and DNA polymerization were initially suggested on kinetic grounds (Rodnina and Wintermeyer, 2001). It is now clear on the structural level that both the 30S subunit and polymerases undergo a rearrangement from an open to a closed form, which interacts intimately with the minor groove of Watson-Crick substrate base pairs. Thus, a common mechanistic principle ensures accurate complementary base-pairing during replication, transcription, and translation of the genetic information.

Experimental Procedures

Structure Determination

T. thermophilus 30S subunits were purified and crystallized as described (Clemons et al., 2001). ASL^{Leu2}, ASL^{Ser}, and the mRNA fragment U_6 were synthesized chemically and gel purified (Dharmacon, USA). Sequences for the ASLs (anticodons underlined; Ψ-pseudouridine) are CUACCUUGAGGΨGGUAG (ASL^{Leu2}) and CACGCCUGGAAAGΨGUG (ASL^{Ser}). 30S crystals were transferred to stabilizing buffer containing 26% 2-methyl-2,4-pentanediol and ligands (300 μM U_6 and 300 μM either ASL^{Leu2} or ASL^{Ser}, each both with and without 80 μM paromomycin) for three days at 4°C, before freezing in liquid nitrogen. X-ray diffraction data were collected at the European Synchrotron Radiation Facility (Grenoble, France), beamline ID14-4, and integrated and scaled using Denzo and Scalepack, version 1.96 (Otwinowski and Minor, 1997). The native 30S subunit coordinates (Wimberly et al., 2000), without the metal ions and with occupancies of regions close to the A site set to zero, were used as a starting model for refinement against the current data sets with CNS (Brünger et al., 1998). 16S RNA domains and proteins were initially refined as separate rigid bodies, followed by positional refinement, simulated annealing with torsional dynamics (to remove possible model bias), and grouped B factor refinement. Ligands and metal ions (where visible) and the omitted regions of 16S RNA, were rebuilt into omit maps using the program O (Jones and Kjeldgaard, 1997) before final positional, B factor, and metal ion occupancy refinement. Figures were made using MolMol (Koradi et al., 1996), or Molscript and Raster3D (Kraulis, 1991; Merritt and Bacon, 1997). Molecular movements were analyzed and compared using ESCET (Schneider, 2002). 16S RNA phosphorus atoms identified as rigid and estimated to have a coordinate error of below 0.2 Å, which were used for least squares superposition of the structures with the program Lsqkab (Collaborative Computational Project 4, 1994), are listed in Supplemental Data (available at http://www.cell.com/cgi/content/full/111/5/721/DC1).

Affinity Assays

T. thermophilus 70S ribosomes were isolated by the same protocol as the 30S, except that sucrose gradient ultracentrifugation and the final hydrophobic interaction chromatography were carried out in 6 mM rather than 2 mM Mg^{2+}. Purified 70S were dialyzed into assay buffer (50 mM Tris·HCl [pH_{20} 7.5], 90 mM NH_4Cl, 50 mM KCl, 10 mM MgOAc, 4 mM 2-mercaptoethanol, 0.1 mM phenyl methyl sulfonyl

fluoride, and 0.1 mM benzamidine), stored at −20°C in aliquots (200 or 400 A_{260}/ml), and heat-activated for 10′ at 50°C before use. A site binding affinities were determined using ^{32}P-labeled ASL^{Phe} (GGGGAUUGAAAAUCCCC), either by homologous competition with unlabeled ASL^{Phe}, for the cognate binding situation, or by heterologous competition with unlabeled ASL^{Leu2} or ASL^{Ser} for near-cognate binding (triplicate samples). 70S ribosomes were first incubated for 10′ at 50°C with a 30–150-fold excess of mRNA (AGGAGGUGAGGU AUGUUUAAA or AGGAGGUGAGGUAUGUUCAAA; A site codons underlined), and initiator tRNA-ASL^{fMet} to block the P site. After addition of paromomycin if required, a constant amount of labeled ASL^{Phe} was added, with varying amounts of unlabeled cognate or near-cognate ASL spanning 5–9 orders of magnitude. Final concentrations in 20 μl assay buffer were: 70S ribosomes: 0.2 μM for assays including paromomycin, 0.5 μM or 1.0 μM without paromomycin; mRNA: 30 μM; ASL^{fMet}: 30 μM; paromomycin (when present): 100 μM; labeled ASL^{Phe}: 60,000 cpm for assays including paromomycin, and 140,000–200,000 cpm without paromomycin (1–60 nM). Samples were first incubated at 50°C for 20′ and then on ice for 1–3 days, to ensure complete equilibration. To measure ribosome-bound, labeled ASL, samples were diluted with 940 μl ice-cold buffer, filtered under vacuum suction on nitrocellulose filters (Schleicher & Schuell, 2.5 cm diameter, 0.45 μm pore size), followed by rapid washing with 3 × 3 ml ice-cold buffer, requiring a maximum of 25 s for dilution, filtration, and washing. The half-life of the labeled cognate ASL on the ribosome measured by dilution experiments (without paromomycin, on codon UUU) was ~100 min. Rebinding of label to A sites vacated by near-cognate ASL after dilution is estimated to be negligible, due to the low concentrations (on the basis of mass action and calculated association rates). Liquid scintillation counting data were fit by nonlinear least squares regression to equations for homologous or heterologous competition with radioligand depletion, using GraphPad Prism version 3.02 for Windows (GraphPad Software, San Diego, California, USA, www.graphpad.com). Values determined from samples with no added cold competitor, and background values without ribosomes (< 3% of maximum values) corresponded well to the upper and lower plateaus of the competition curves, respectively, and were added to the data at low (10^{-15} M) and high (10 M) concentration extremes, respectively, for regression analysis.

Acknowledgments

We thank G. Sainz and R. Ravelli for help with data collection at the ESRF; M. Ehrenberg for suggesting the competition binding method; A.P. Carter for valuable advice and discussions throughout this work; R.L. Williams, H.F. Noller, D. Turner, K. Nagai, P.J.G. Butler, and R. Gillet for comments on the manuscript. J.M.O. was supported by a PhD scholarship of the Boehringer Ingelheim Fonds (Germany). This work was funded by the Medical Research Council (UK) and NIH grant GM 44973 to S.W. White and V.R.

Received: July 10, 2002
Revised: September 26, 2002

References

Bartlett, P.A., and Marlowe, C.K. (1987). Evaluation of intrinsic binding energy from a hydrogen bonding group in an enzyme inhibitor. Science *235*, 569–571.

Battle, D.J., and Doudna, J.A. (2002). Specificity of RNA-RNA helix recognition. Proc. Natl. Acad. Sci. USA *99*, 11676–11681.

Brünger, A.T., Adams, P.D., Clore, G.M., DeLano, W.L., Gros, P., Grosse-Kunstleve, R.W., Jiang, J.S., Kuszewski, J., Nilges, M., Pannu, N.S., et al. (1998). Crystallography & NMR system: a new software suite for macromolecular structure determination. Acta Crystallogr. *D54*, 905–921.

Carter, A.P., Clemons, W.M.J., Brodersen, D.E., Morgan-Warren, R.J., Wimberly, B.T., and Ramakrishnan, V. (2000). Functional insights from the structure of the 30S ribosomal subunit and its interactions with antibiotics. Nature *407*, 340–348.

Cheetham, G.M., and Steitz, T.A. (2000). Insights into transcription: structure and function of single-subunit DNA-dependent RNA polymerases. Curr. Opin. Struct. Biol. *10*, 117–123.

Chen, X., McDowell, J.A., Kierzek, R., Krugh, T.R., and Turner, D.H. (2000). Nuclear magnetic resonance spectroscopy and molecular modeling reveal that different hydrogen bonding patterns are possible for G.U. pairs. Biochemistry *39*, 8970–8982.

Clemons, W.M.J., May, J.L., Wimberly, B.T., McCutcheon, J.P., Capel, M.S., and Ramakrishnan, V. (1999). Structure of a bacterial 30S ribosomal subunit at 5.5 A resolution. Nature *400*, 833–840.

CCP4 (Collaborative Computational Project 4) (1994). The CCP4 suite: programs for protein crystallography. Acta Crystallogr. *D50*, 760–763.

Clemons, W.M., Jr., Brodersen, D.E., McCutcheon, J.P., May, J.L., Carter, A.P., Morgan-Warren, R.J., Wimberly, B.T., and Ramakrishnan, V. (2001). Crystal structure of the 30 S ribosomal subunit from *Thermus thermophilus*: purification, crystallization and structure determination. J. Mol. Biol. *310*, 827–843.

Crick, F.H.C. (1966). Codon-anticodon pairing: the wobble hypothesis. J. Mol. Biol. *19*, 548–555.

Davies, J., Gilbert, W., and Gorini, L. (1964). Streptomycin, suppression, and the code. Proc. Natl. Acad. Sci. USA *51*, 883–890.

Doherty, E.A., Batey, R.T., Masquida, B., and Doudna, J.A. (2001). A universal mode of helix packing in RNA. Nat. Struct. Biol. *8*, 339–343.

Eisinger, J., Feuer, B., and Yamane, T. (1971). Codon-anticodon binding in tRNAphe. Nat. New Biol. *231*, 126–128.

Fourmy, D., Recht, M.I., Blanchard, S.C., and Puglisi, J.D. (1996). Structure of the A site of *Escherichia coli* 16S ribosomal RNA complexed with an aminoglycoside antibiotic. Science *274*, 1367–1371.

Glukhova, M.A., Belitsina, N.V., and Spirin, A.S. (1975). A study of codon-dependent binding of aminoacyl-tRNA with the ribosomal 30-S subparticle of *Escherichia coli*. Determination of the active-particle fraction and binding constants in different media. Eur. J. Biochem. *52*, 197–202.

Grosjean, H.J., de Henau, S., and Crothers, D.M. (1978). On the physical basis for ambiguity in genetic coding interactions. Proc. Natl. Acad. Sci. USA *75*, 610–614.

Herschlag, D. (1988). The role of induced fit and conformational changes in specificity and catalysis. Bioorg. Chem. *16*, 62–96.

Hopfield, J.J. (1974). Kinetic proofreading: a new mechanism for reducing errors in biosynthetic processes requiring high specificity. Proc. Natl. Acad. Sci. USA *71*, 4135–4139.

Jones, T.A., and Kjeldgaard, M. (1997). Electron-density map interpretation. Meth. Enzymol. *277B*, 173–207.

Kool, E.T. (2002). Active site tightness and substrate fit in DNA replication. Annu. Rev. Biochem. *71*, 191–219.

Koradi, R., Billeter, M., and Wüthrich, K. (1996). MOLMOL: a program for display and analysis of macromolecular structures. J. Mol. Graph. *14*, 51–55.

Kraulis, P. (1991). MOLSCRIPT: A program to produce both detailed and schematic plots of protein structures. J. Appl. Crystallogr. *24*, 946–950.

Kunkel, T.A., and Bebenek, K. (2000). DNA replication fidelity. Annu. Rev. Biochem. *69*, 497–529.

Kurland, C.G., Hughes, D., and Ehrenberg, M. (1996). Limitations of translational accuracy. In *Escherichia coli* and *Salmonella typhimurium*: Cellular and Molecular Biology, F.C. Neidhardt, Curtiss, R. III, Ingraham, J.L., Lin, E.C.C., Low, K.B., Magasanik, B., eds. (Washington, DC: American Society for Microbiology Press), pp. 979–1004.

Lim, V.I., and Curran, J.F. (2001). Analysis of codon: anticodon interactions within the ribosome provides new insights into codon reading and the genetic code structure. RNA *7*, 942–957.

Lodmell, J.S., and Dahlberg, A.E. (1997). A conformational switch in *Escherichia coli* 16S ribosomal RNA during decoding of messenger RNA. Science *277*, 1262–1267.

Mathews, D.H., Sabina, J., Zuker, M., and Turner, D.H. (1999). Expanded sequence dependence of thermodynamic parameters improves prediction of RNA secondary structure. J. Mol. Biol. *288*, 911–940.

Merritt, E.A., and Bacon, D.J. (1997). Raster3D: photorealistic molecular graphics. Meth. Enzymol. *277*, 505–524.

Nierhaus, K.H. (1990). The allosteric three-site model for the ribosomal elongation cycle: features and future. Biochemistry *29*, 4997–5008.

Ninio, J. (1975). Kinetic amplification of enzyme discrimination. Biochimie *57*, 587–595.

Nissen, P., Ippolito, J.A., Ban, N., Moore, P.B., and Steitz, T.A. (2001). RNA tertiary interactions in the large ribosomal subunit: the A-minor motif. Proc. Natl. Acad. Sci. USA *98*, 4899–4903.

Ogle, J.M., Brodersen, D.E., Clemons, W.M., Jr., Tarry, M.J., Carter, A.P., and Ramakrishnan, V. (2001). Recognition of cognate transfer RNA by the 30S ribosomal subunit. Science *292*, 897–902.

Otwinowski, Z., and Minor, W. (1997). Processing of x-ray diffraction data collected in oscillation mode. In Methods Enzymol., C.W.J. Carter, and R. M. Sweet, eds. (New York: Academic Press), pp. 307–325.

Pape, T., Wintermeyer, W., and Rodnina, M. (1999). Induced fit in initial selection and proofreading of aminoacyl-tRNA on the ribosome. EMBO J. *18*, 3800–3807.

Piepenburg, O., Pape, T., Pleiss, J.A., Wintermeyer, W., Uhlenbeck, O.C., and Rodnina, M.V. (2000). Intact aminoacyl-tRNA is required to trigger GTP hydrolysis by elongation factor Tu on the ribosome. Biochemistry *39*, 1734–1738.

Pongs, O., Bald, R., and Reinwald, E. (1973). On the structure of yeast tRNAPhe. Complementary-oligonucleotide binding studies. Eur. J. Biochem. *32*, 117–125.

Powers, T., and Noller, H.F. (1994). Selective perturbation of G530 of 16 S rRNA by translational miscoding agents and a streptomycin-dependence mutation in protein S12. J. Mol. Biol. *235*, 156–172.

Rodnina, M.V., and Wintermeyer, W. (2001). Fidelity of aminoacyl-tRNA selection on the ribosome: kinetic and structural mechanisms. Annu. Rev. Biochem. *70*, 415–435.

Rodnina, M.V., Fricke, R., and Wintermeyer, W. (1994). Transient conformational states of aminoacyl-tRNA during ribosome binding catalyzed by elongation factor Tu. Biochemistry *33*, 12267–12275.

Schluenzen, F., Tocilj, A., Zarivach, R., Harms, J., Gluehmann, M., Janell, D., Bashan, A., Bartels, H., Agmon, I., Franceschi, F., and Yonath, A. (2000). Structure of functionally activated small ribosomal subunit at 3.3 Å resolution. Cell *102*, 615–623.

Schneider, T.R. (2002). A genetic algorithm for the identification of conformationally invariant regions in protein molecules. Acta Crystallogr. D Biol. Crystallogr. *58*, 195–208.

Seeman, N.C., Rosenberg, J.M., and Rich, A. (1976). Sequence-specific recognition of double helical nucleic acids by proteins. Proc. Natl. Acad. Sci. USA *73*, 804–808.

Thompson, R.C., and Stone, P.J. (1977). Proofreading of the codon-anticodon interaction on ribosomes. Proc. Natl. Acad. Sci. USA *74*, 198–202.

Thompson, R.C., and Dix, D.B. (1982). Accuracy of protein biosynthesis. A kinetic study of the reaction of poly(U)-programmed ribosomes with a leucyl-tRNA2-elongation factor Tu-GTP complex. J. Biol. Chem. *257*, 6677–6682.

Uhlenbeck, O.C., Martin, F.H., and Doty, P. (1971). Self-complementary oligoribonucleotides: effects of helix defects and guanylic acid-cytidylic acid base pairs. J. Mol. Biol. *57*, 217–229.

Valle, M., Sengupta, J., Swami, N.K., Grassucci, R.A., Burkhardt, N., Nierhaus, K.H., Agrawal, R.K., and Frank, J. (2002). Cryo-EM reveals an active role for aminoacyl-tRNA in the accommodation process. EMBO J. *21*, 3557–3567.

VanLoock, M.S., Agrawal, R.K., Gabashvili, I.S., Qi, L., Frank, J., and Harvey, S.C. (2000). Movement of the decoding region of the 16 S ribosomal RNA accompanies tRNA translocation. J. Mol. Biol. *304*, 507–515.

Wimberly, B.T., Brodersen, D.E., Clemons, W.M., Morgan-Warren, R.J., Carter, A.P., Vonrhein, C., Hartsch, T., and Ramakrishnan, V. (2000). Structure of the 30S ribosomal subunit. Nature *407*, 327–339.

Xia, T., SantaLucia, J., Jr., Burkard, M.E., Kierzek, R., Schroeder, S.J., Jiao, X., Cox, C., and Turner, D.H. (1998). Thermodynamic parameters for an expanded nearest-neighbor model for formation of RNA duplexes with Watson-Crick base pairs. Biochemistry *37*, 14719–14735.

Yarus, M., and Smith, D. (1995). tRNA on the ribosome: a waggle theory. In tRNA: Structure, Biosynthesis and Function, D. Söll, and U. RajBhandary, eds. (Washington: American Society for Microbiology), pp. 443–468.

Yusupov, M.M., Yusupova, G.Z., Baucom, A., Lieberman, K., Earnest, T.N., Cate, J.H., and Noller, H.F. (2001). Crystal structure of the ribosome at 5.5 A resolution. Science *292*, 883–896.

Accession Numbers

Accession numbers for coordinates deposited at the Protein Data Bank are 1N34 (30S:U_6:ASL^{Leu2}), 1N32 (30S:U_6:ASL^{Leu2}:paromomycin), 1N36 (30S:U_6:ASL^{Ser}), and 1N33 (30S:U_6:ASL^{Ser}:paromomycin).